The International Journal of Advanced Manufacturing Technology (2019) 102:497–505
https://doi.org/10.1007/s00170-018-3197-x

ORIGINAL ARTICLE

Effect of the pressure on fracture behaviors of metal sheet punched by laser-induced shock wave

Min Li[1] · Xingquan Zhang[1] · Shengzhi Li[2] · Huiting Wang[2] · Bin Chen[1] · Jinyu Tong[1] · Guangwu Fang[1] · Wei Wei[1]

Received: 18 June 2018 / Accepted: 12 December 2018 / Published online: 4 January 2019

Abstract
Two laser-induced shock wave pressures, 4.5 and 6.5 GPa, were applied to punch LC4CS aluminum sheet respectively, and the influence of different pressures on fracture behaviors was investigated. The code ANSYS/LS-DYNA, dynamic finite element software, was employed to investigate the sheet fracture behaviors during the punching process. The experimental results display that the punching quality manufactured by higher peak pressure of shock wave is better than that by lower one. The finite element method visualizes the punching process, including sheet deformation, cracks growth, and plug flying away. The computational analysis results reveal that the time to punch the sheet with higher peak pressure of shock wave is shorter than that with lower one, and the edge of punched hole resulted from the higher peak pressure is smoother than that from the lower one, which are consistent well with the experimental results.

Keywords Laser · Shock wave · Pressure · Punch · Quality

1 Introduction

Laser shock sheet forming [1–5] has been gaining more and more attentions due to the advantages of its flexibility, repeatability, simplicity, and precision. During laser shock sheet forming, the metal fails if the pressure of the loaded shock wave is too high [6–8]. For example, Li et al. [7] investigated the maximum forming limit and fracture of thin films impacted by laser. Zheng et al. [8] probed the fracture mechanism of $Fe_{78}Si_9B_{13}$ metallic glass impacted by laser under different conditions. Liu et al. [9, 10] utilized single-laser pulse to drive a flyer to punch three holes in pure copper sheet at one time. Prior to these researches, Zhou and Zhang presented the concept of laser punching, which utilizes laser-induced shock wave to punch metal sheet to obtain a hole [11], which is different from laser drilling that uses the high-energy laser to ablate metal material directly. Therefore, laser shock wave punching has no drawbacks that laser drilling possesses, which seriously damage the quality of the workpiece. Compared with the traditional microdrilling, the laser punching can avoid sheet wrinkle and cutter wear, so this novel technology can meet the needs of microhole in aerospace, microelectronics, medical apparatus, and instruments. However, up to now, there have been few references about laser punching, and its characteristics have not been well known, so it is worth investigation.

The aim of the paper was to simulate the dynamic process of sheet punched by laser-induced shock wave with software

✉ Xingquan Zhang
zhang20020313@163.com

Min Li
Leem0828@163.com

Shengzhi Li
lisz55@ahut.edu.cn

Huiting Wang
htwang@ahut.edu.cn

Bin Chen
chenbinahut@163.com

Jinyu Tong
994115013@qq.com

Guangwu Fang
403291736@qq.com

Wei Wei
5734237@qq.com

[1] School of Mechanical Engineering, Anhui University of Technology, Ma'anshan 243032, Anhui, China

[2] School of Metallurgy Engineering, Anhui University of Technology, Ma'anshan 243032, Anhui, China

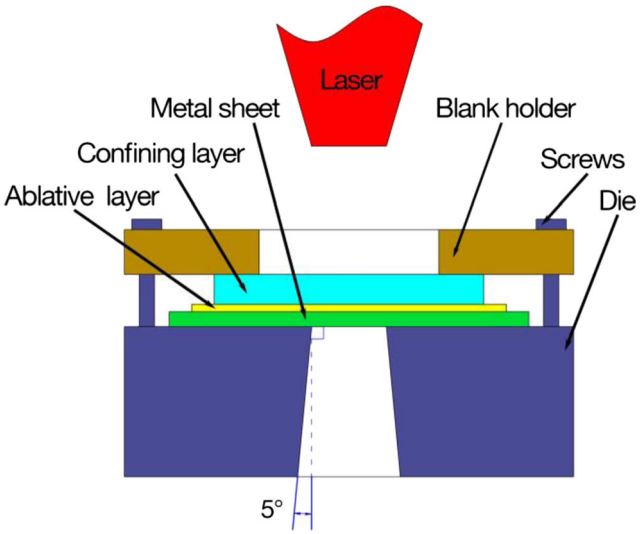

Fig. 1 Schematic of punching sheet

ANSYS/LS-DYNA, and the effects of different shock wave pressures on the sheet punching behaviors were investigated, including quality of punching, energy obtained from shock wave, sheet deforming velocity, strain, and completion time of punching. The experimental tests were carried out to validate the predicted results. The fracture modes induced by the different peak pressures of shock waves were also presented and discussed.

2 Punching mechanism

As illustrated in Fig. 1, the top surface of metal sheet is successively covered with an ablative coating and a confining coating, and the coated sheet is placed upon the punching die and fixed with blank holder and screws. Laser beam travels through a transparent confining coating and irradiates vertically onto the surface of opaque ablative coating. Then, the ablative coating evaporates and is ionized into plasma with high temperature and high pressure instantaneously. The expansion of high pressure plasma results in generating shock wave and is delayed by the confining coating. The metal sheet is subjected to the high-pressure shock wave and obtains the momentum and kinetic energy from the loaded shock wave, so the central unsupported part of metal sheet moves downward into the die rapidly. The central rapidly moving part is sheared off from the matrix by the die to form a plug, which flies away. As a result, a hole is left in the sheet.

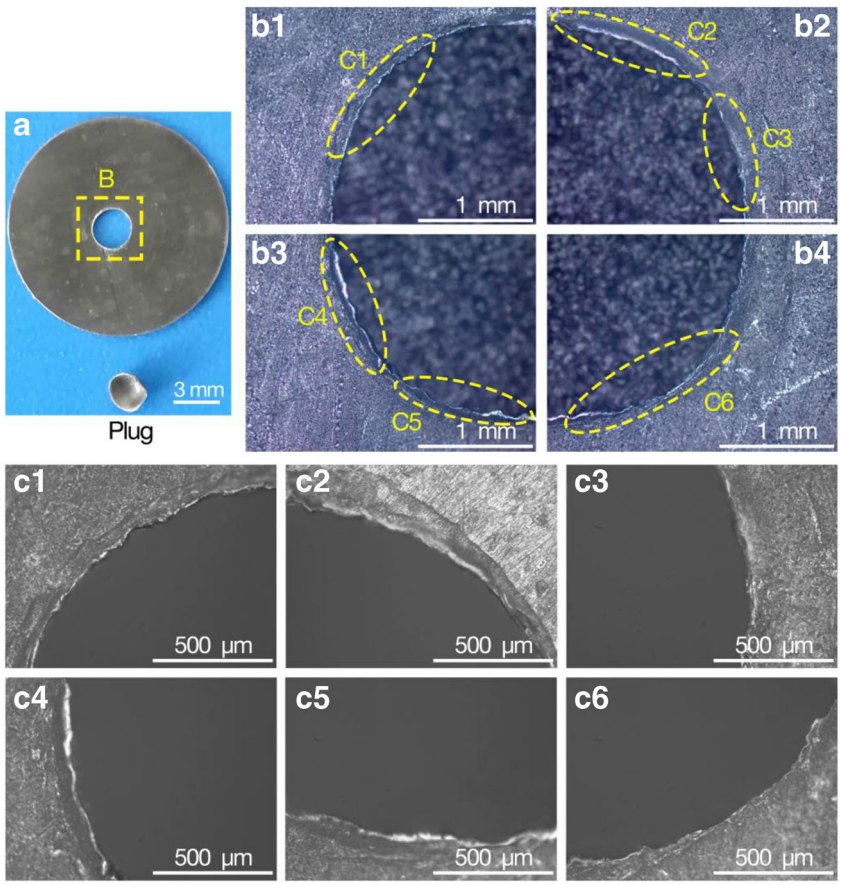

Fig. 2 Fracture surface morphology of sample punched by pressure of shock wave 4.5 GPa. a Views of the punched hole and plug. b1, b2, b3, b4 General views of the fracture region B in a. c1, c2, c3, c4, c5, c6 Amplifications of corresponding regions in b1, b2, b3, and b4, respectively

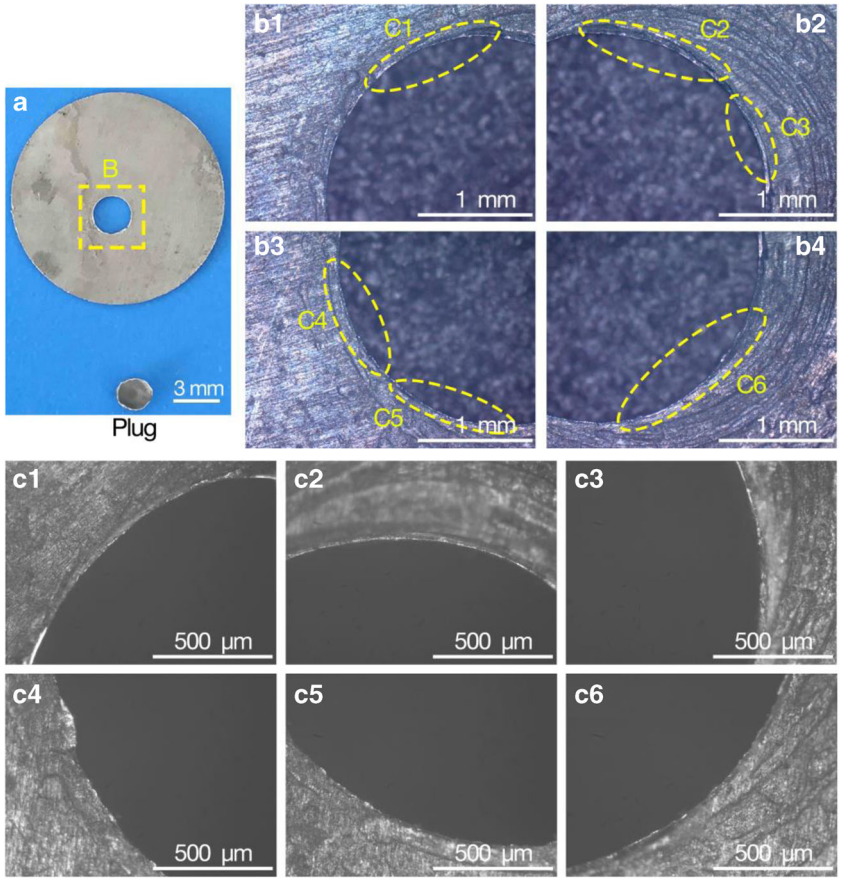

Fig. 3 Fracture surface morphology of sample punched by pressure of shock wave 6.5 GPa. a Views of the punched hole and plug. b1, b2, b3, b4 General views of the fracture region B in a. c1, c2, c3, c4, c5, c6 Amplifications of corresponding regions in b1, b2, b3, and b4, respectively

3 Experiments

The punched specimens were LC4CS aluminum sheet with 15 mm in diameter, and the material chemical composition (wt.%) was Mn 0.2–0.6, Cr 0.1–0.25, Zn 5.0–7.0, Mg 1.8–2.8, Cu 1.4–2.0, Si 0.5, Fe 0.5, Al Margin. Its mechanical properties were as follows, tensile strength σ_b 620 MPa, proportional limit σ_p 430 MPa, hardness 150 HB. The samples were cut from the rolled bar with a diameter of 20 mm through lathe tool cutting. The surfaces of the sample were polished orderly by SiC papers with grit number 400, 800, and 1200 to reduce its surface roughness. When the thickness was decreased to 0.1 mm, the operation of polishing ends. Subsequently, the samples were cleaned with anhydrous alcohol and dried in air. Prior to laser irradiating, a special Al foil was pasted onto sample surface to serve as an ablative coating. K9 glass with a thickness of 4.5 mm was used to cover the ablative coating and to serve as the confining coating. Thus, the experimental assembly consisted of target sheet, ablative foil, and K9 glass. In order to ensure that each item was in its exact position during stamping process, all these items were pressed tightly by a blank holder with a central hole diameter of 5 mm onto the punching die, whose opening was 2.6 mm in diameter and inclined angle of die cavity wall was 5°. A YAG laser was adopted to emit laser pulse, and the parameters were as follows: the pulse duration of full width at half maximum about 20 ns, wavelength 1064 nm, local laser spot 2.6 mm in diameter, and each pulse energy varied according to the needs that generate the desired pressure. In the current case, the metal sheets were shocked by once-laser pulse with energy about 3.5 and 8.0 J respectively.

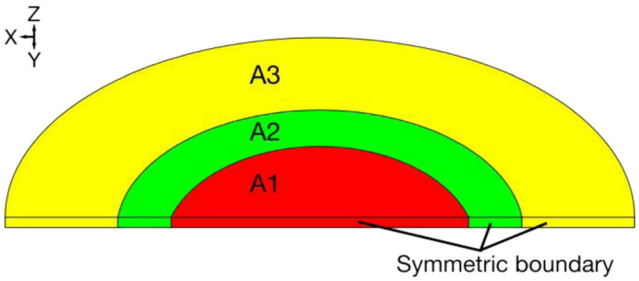

Fig. 4 Schematic diagram of model region division

After shocking, the residual coating ablated by laser was removed from the sample, and the punched sample was washed with acetone, and the detached plug was also collected. Figures 2(a) and 3(a) show the appearances of the plug and the punched hole resulted from the different pressures. The optical microscope was adopted to observe the surface morphology of the hole. In order to see the microscopic appearance clearly, the hole is magnified. Since the view field of the

Table 1 Physical and mechanical properties of LC4CS [20]

Material	ρ (kg/m^3)	E (GPa)	ν	σ_0(GPa)	E_{tan} (GPa)	β	C	P
LC4CS	2850	70.1	0.33	0.43	2.29	1	34,295.5	1.904

optical microscope cannot cover the whole hole magnified by 50 and 100 times, the punched hole was intentionally divided into several parts. The local enlarged parts of the hole resulted from different peak pressures are shown in Figs. 2(b1~b4) and 3(b1~b4) respectively. Figures 2(c1~c6) and 3(c1~c6) are further magnified diagrams, which correspond to the marked regions in Figs. 2(b1~b4) and 3(b1~b4) respectively.

From Figs. 2(a) and 3(a), it can be seen that the material within the die cavity has been punched, and a hole emerges at the center of metal sheet, whose diameter equals to the opening diameter of die. The specimen after punching still keeps flat, and there is few turned-down edge. The shapes of the formed plugs are different under different pressure conditions. The plug punched by the peak pressure of 4.5 GPa looks like an intact spherical cap, while the other plug punched by the pressure 6.5 GPa is an irregular cap. Moreover, the height of the spherical cap is about 0.9 mm which is resulted from the peak pressure 4.5 GPa, while it is roughly 0.6 mm resulted from 6.5 GPa. From the magnified pictures in Figs. 2 and 3, it can be seen that the punched hole resulted from pressure 4.5 GPa has a sharp saw tooth edge, while the hole resulted from pressure 6.5 GPa has a relatively smooth edge, which implies that the quality of the hole fabricated by higher pressure is better than that by the lower one.

4 Numerical simulation

The software ANSYS/LS-DYNA with the basic explicit algorithm, and ALE advanced algorithm was widely used in impact dynamic analysis in practice [12–15]. In order to directly compare the results, the size of finite element model is identical with experimental sample size, and a half finite element model was established to save calculation cost, as demonstrated in Fig. 4. According to experimental physical model, the red area A1 in Fig. 4 was the shocked region with diameter 2.6 mm, and the green area A2 was a deformation transition region with diameter 4 mm, and the displacement along the Z axis direction of nodes at the bottom surface was constrained. The outermost yellow area A3 was a constricted region with diameter 15 mm, whose nodes on both side surfaces were fully constrained. The symmetric boundary was employed in symmetric surface. An element type of solid164 was chosen to mesh sheet target. The element lengths along the radius direction in regions A1, A2, and A3 were 0.03 mm, 0.015 mm, and 0.05 mm, respectively, and the element height along the sheet thickness was 0.02 mm in all regions. The model could be easily meshed into a five-layer finite element set along sheet thickness, and there were 435,290 elements in all and 525,192 nodes in the developed model.

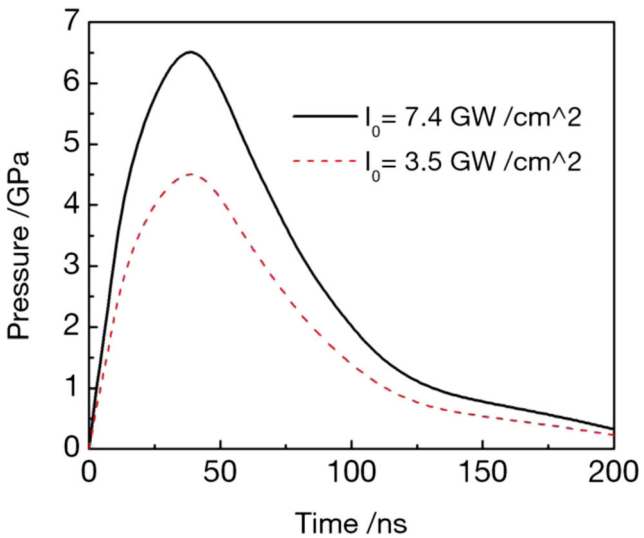

Fig. 5 Loading curves of shock wave pressure

4.1 Material constitutive model

In the laser shocking process, metal sheet is subjected to the pressure of GPa magnitude level instantaneously. Due to the ultra-short time of interaction between the material and laser, the material strain rate is up to 10^5 s^{-1} [16]. The Cowper-Symonds material model is commonly used to express the material response at high strain rate [17–19], and the dynamic yield stress is defined as [17–19]:

$$\sigma_Y = \left[1 + \left(\frac{\dot{\varepsilon}}{C}\right)^{\frac{1}{P}}\right]\left(\sigma_0 + \beta E_p \varepsilon_p^n\right) \quad (1)$$

$$E_p = \frac{E_{\tan} \bullet E}{(E - E_{\tan})} \quad (2)$$

where σ_Y is the effective flow stress, C and P are the parameters used to describe the strain-rate effect of the material, $\dot{\varepsilon}$ stands for the plastic strain rate, σ_0 denotes the initial yield stress of material, β is the strain-hardening coefficient, ε_P stands for the plastic strain, n is the strain-hardening exponent, and E_p is the plastic hardening modulus which originates from the tangent modules E_{tan} and the elastic modulus E, as illustrated in Eq. (2). The required parameters in Cowper-Symonds model of LC4CS aluminum material were shown in Table 1 [20].

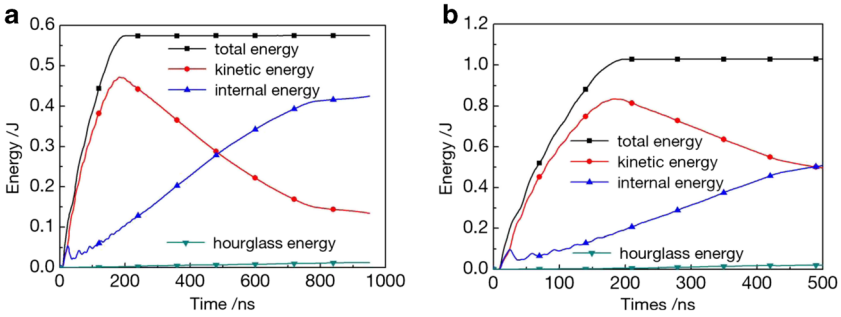

Fig. 6 Time history of energy under two different laser shock wave pressures. **a** 4.5 GPa. **b** 6.5 GPa

4.2 Loading

The loading of laser-induced shock wave pressure on metal sheet is one of the key influencing factors in simulation. Because of adopting the confining model, the shock duration is 2~3 times longer than that of the excited laser pulse [21]. According to Fabbro' s developed model, the relationship between the peak pressure of shock wave and power density of laser pulse is expressed as follows [21]:

$$P = 0.01\sqrt{\alpha/(2\alpha+3)}\sqrt{\mathrm{ZI}_0} \tag{3}$$

$$2/\mathrm{Z} = 1/\mathrm{Z}_1 + 1/\mathrm{Z}_2 \tag{4}$$

where P is the peak pressure of shock wave, α is the coefficient of internal energy dedicated to thermal energy and is set to be 0.15 [22], and I_0 is the power density of the applied laser. Z is the equivalent shock impedance of the confining layer and the ablative layer, as shown in Eq. (4), and the subscripts, 1 and 2, stand for the confining coating material and the ablative coating material respectively ($Z_1 = 1.14 \times 10^6$ g/cm^2 s, $Z_2 = 1.38 \times 10^6$ g/cm^2 s). According to the adopted energy values of 3.5 and 8.0 J in previous experiments, the corresponding laser power densities are 3.5 and 7.4 GW/cm^2, which can induce the shock wave with peak pressure of 4.5 and 6.5 GPa respectively according to the above-mentioned formula. The fitting pressure profiles were plotted in the following Fig. 5. The finite element program uses the interpolation algorithm to calculate the pressure at any time and loads it onto the specified area.

4.3 Failure strain

It is vital to set a threshold value of material failure strain in C-S failure model. During calculation, once the threshold value is satisfied, the elements would fail, which are automatically deleted from the subsequent calculation by activating element deletion algorithm available in software, and the stress

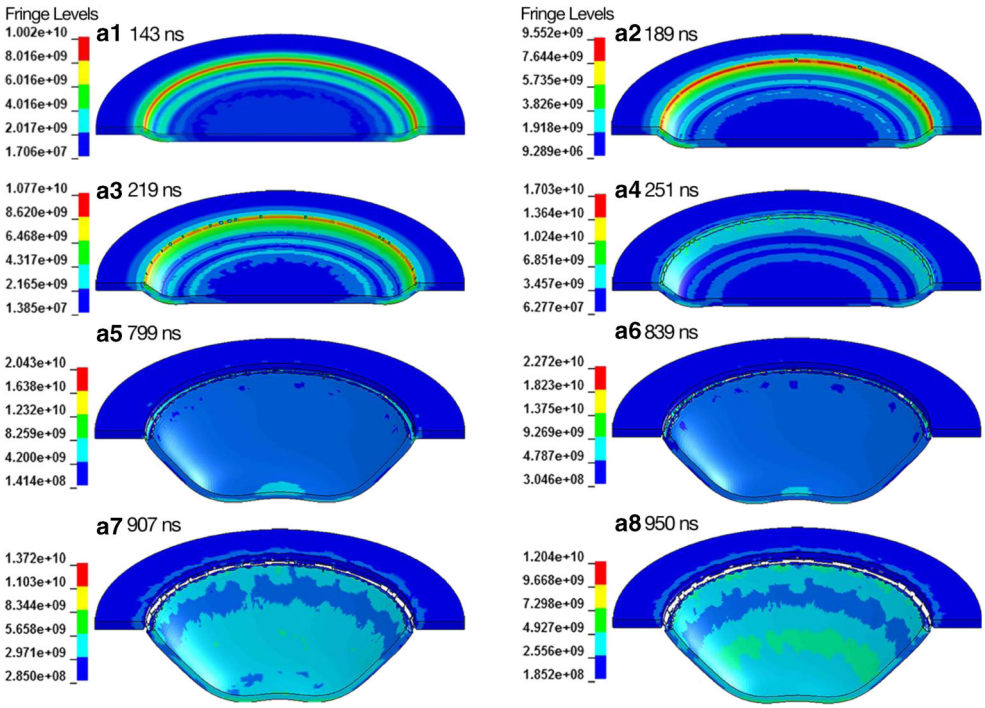

Fig. 7 Contour of the Von Mises under different pressures. a1~a8 4.5 GPa. b1~b8 6.5 GPa

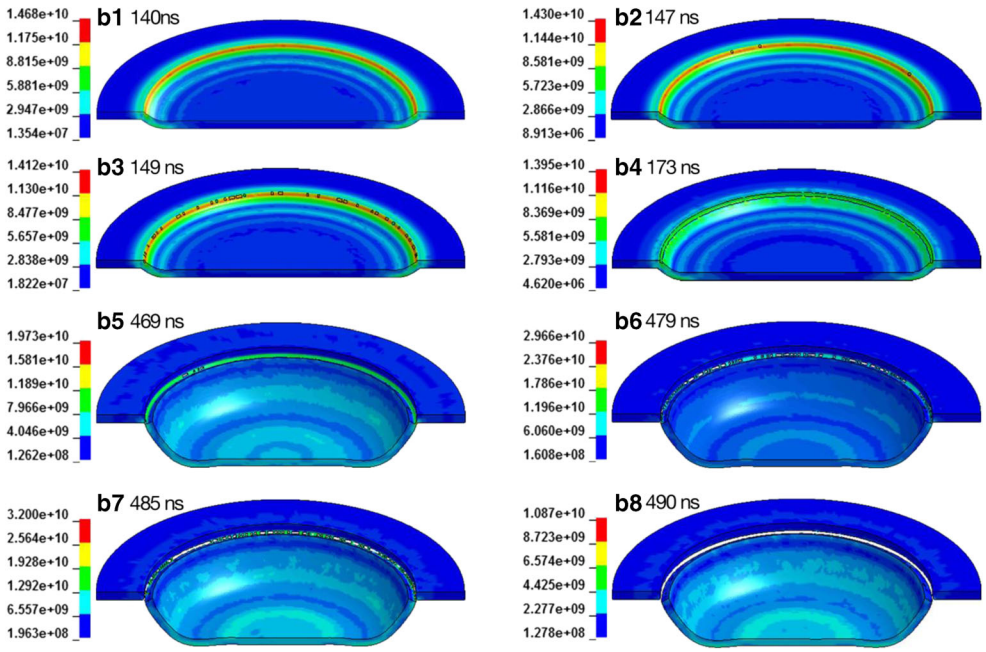

Fig. 7 continued.

resulted from the applied pressure in deleted elements also vanishes during the next analysis. A widely used method is to pre-set the threshold value in advance to proceeding simulation, and then the obtained predicted result is compared with experimental result under the same condition. The preset value is continuously adjusted until the calculated result accords with experimental result, and the preset value is served as the threshold value [23, 24]. In the current situation, the threshold value of failure strain is also determined by coupling computational and experimental results based on the stress-strain curve of LC4CS aluminum alloy in references [18, 25], and the threshold values failure strain are finally set to be 0.33 and 0.35 respectively, which correspond to the conditions of two different peak pressures 4.5 and 6.5 GPa.

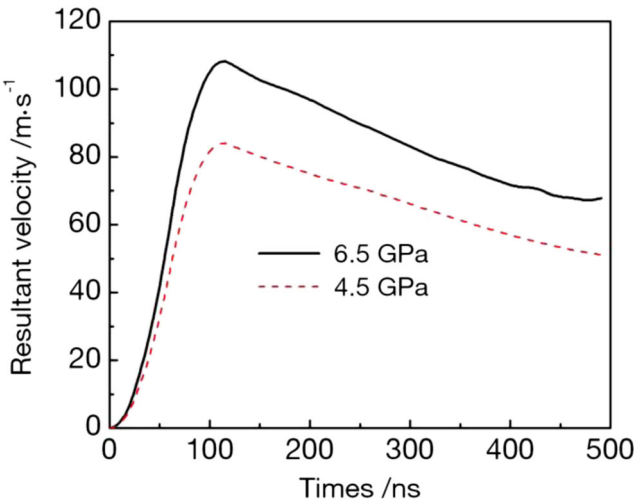

Fig. 8 The velocity history of the center element under two different pressures

5 Numerical results

5.1 Energies

When the pressure pulse induced by shock wave is imposed on metal sheet, the sheet obtains energy from the shock wave, which subsequently transfers into kinematic energy, internal energy, and so on step by step. Figure 6 demonstrates the curves of energy versus time, which are output from the file of *d3plot* in LS-PrePost according to calculation results.

From Fig. 6, it can be seen that the total energy obtained from shock wave increases and rapidly reaches its maximum and keeps constant. Kinematic energy instantly increases in initial stage and then gradually decreases, and internal energy initially increases and, afterwards, almost remains unchanged. Once the sheet gains energy from the imposed shock wave, it moves rapidly at high speed, and the metal sheet deforms, so the obtained energy initially transfers into kinematic energy. With the increasing of sheet deformation, the velocity of sheet decreases and plastic work increases, so kinematic energy decreases and transfers into internal energy, so the internal energy increases. The internal energy includes the irreversible plastic work and the stored reversible elastic energy, and the release of stored elastic energy in deformed sheet will lead to the velocity enhancement of the sheet, so small fluctuation of velocity occurs during the process of kinematic energy attenuation and internal energy increase. In the calculation of

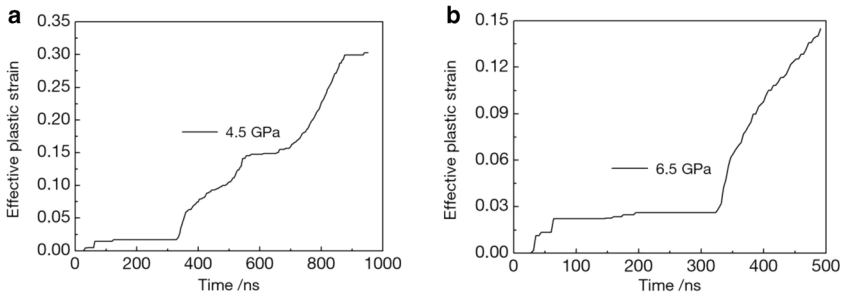

Fig. 9 Time history of strain under two different laser shock wave pressures. **a** 4.5 GPa. **b** 6.5 GPa

Abaqus Explict, a tiny quantity of artificial hourglass stiffness is employed to restrict the transmission of hourglass modes in first-order reduced integration elements. Hourglass energy, approximately 2% of the total internal energy, is to control hourglass deformation, which indicates that mesh refinement is acceptable [26].

From Fig. 6, it can also be seen that the hourglass energy is below 5% total energy, which validates the developed model. Comparing kinematic energy of metal sheet obtained from shock wave with different pressures, it can be found that the sheet obtains energy 0.80 J from shock wave with peak pressure 6.5 GPa, which is bigger than 0.45 J from shock wave with 4.5 GPa. So, the velocity of sheet impacted by pressure 6.5 GPa is faster than that by pressure 4.5 GPa.

5.2 Dynamic punching process

Figure 7 shows the process of aluminum alloy sheet punched by shock wave. In order to see clearly, only the marked areas A1 and A2 in Fig. 4 are displayed and magnified during the fracture process. Figure 7(a1~a8) show the process of sheet punched by pressure 4.5 GPa at typical times. And Fig. 7(b1~b8) are the process of sheet punched by pressure 6.5 GPa. From Fig. 7(a1~a8), as can be viewed, at 143 ns, the dynamic deformation occurred. At 189 ns, two microcracks initiate in the edge of the deforming area. With time going on, more microcracks form, and microcracks grow and coalesce along the circumferential direction to form long cracks. At 907 ns, the cracks penetrate through the thickness at some regions of the circular edge. Subsequently, the cracks continue expanding and gradually connect to each other into an entire crack along the edge of the circumference. At 950 ns, the material within the die is punched off from the matrix, and the plug is formed and flies away. Thus, a hole is formed in the sheet.

The process of sheet punched by pressure 6.5 GPa is similar to that by 4.5 GPa, as shown in Fig. 7(b1~b8). The metal sheet first undergoes plastic deformation. At 147 ns, three crack initiations are found at the edge of the deformation area. Then, more crack initiations are generated, and microcracks expand and coalesce. At 490 ns, the plug breaks away from the matrix, and the punching process is completed.

Comparing the processes of sheet punched by two different pressures, the time to complete punching with pressure 4.5 GPa is 950 ns, while the time for pressure 6.5 GPa is 490 ns. Obviously, the time of punching with the higher pressure is shorter than that with the lower one. Because of having more time, the plug punched by 4.5 GPa experiences adequate plastic deformation and has a deeper depth, while the plug punched by 6.5 GPa has not enough time to fulfill the plastic deformation and has a shallower depth. Moreover, the edge of hole punched by 6.5 GPa is smooth in comparison with that by 4.5 GPa. These computed results are consistent with the physical findings.

5.3 Velocities

Figure 8 illustrates the velocity change of the central node of metal sheet during the punching process. Under the shock wave pressure, the velocity rapidly runs up to the maximum value with ultra-short time, and then gradually decreases. Although two shock waves possess identical duration, the

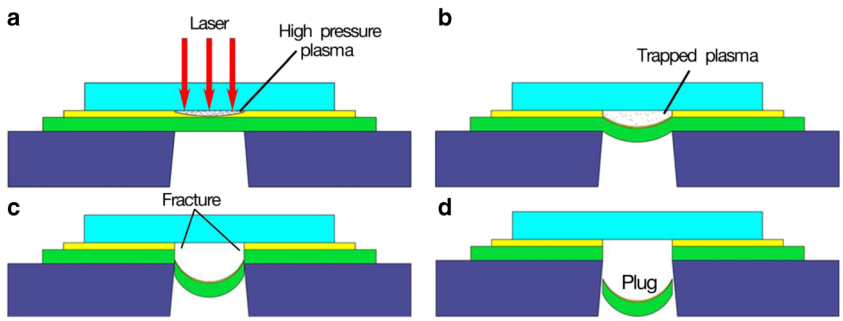

Fig. 10 Schematic of laser shock punching process. **a** High pressure plasma generation. **b** Sheet deformation. **c** Crack growth. **d** Plug forming

peak pressures are different. The shock wave with peak pressure 6.5 GPa imparts more energy and bigger momentum to the sheet in comparison with the shock wave with 4.5 GPa, so its velocity is bigger, and the maximum reaches 108 m/s, while the maximum value is 83 m/s in the case of 4.5 GPa. Due to the adopted material with higher yield stress limit and crack growth consuming a great deal of energy, the maximum velocity in the current case is relatively lower in comparison with the maximum value in laser shock forming [27].

5.4 Strain and strain rate

Figure 9 shows the time-strain relationship of the selected element at the center of shocked region under two different pressures respectively. From Fig. 9, it can be seen that the equivalent plastic strain generally increases in the initial stage and remains constant for several time intervals, which may be attributed to temporarily reverse yielding because of the focus of surface tensile stress waves. The strain rate can be calculated according to strain increment within the execution time. For sheet shocked by pressure 4.5 GPa, the increment of strain is 0.30 and the persisting time is 950 ns according to Fig. 9, so the average strain rate is roughly $3.15 \times 10^5\ s^{-1}$. For sheet with pressure of 6.5 GPa, the increment of strain is 0.15 and the corresponding completing persisting time is 490 ns, so the calculated strain rate is up to $3.06 \times 10^5\ s^{-1}$. Therefore, the strain rate of the target material under 4.5 GPa pressure is similar to that of the target subjected to 6.5 GPa pressure. The current strain rate with the magnitude of $10^5\ s^{-1}$ is consistent with previous research result [28, 29]. It needs to point out that the material strain rate becomes greater when the persisting time does not include the time of strain keeping constant.

6 Discussion

When laser irradiates the ablative layer and induces shock wave, the high-pressure pulse of shock wave is exerted on metal sheet instantly. The shock wave imparts momentum and energy to metal sheet to make it move rapidly and leads to irreversible plastic deformation of metal sheet.

Because of the restriction from blank holder, sheet material at the edge of punching die cavity entrance is pulled off by others which are deformed into the die cavity with high velocity, and undergoes stretching, bending, shearing, and necking, so the maximum stress occurs at this region, and greater stress occurs at impurities in material in this region due to stress concentration. If the tensile stress at this region goes beyond the fracture strength, the impurities including grain boundaries, inclusions, and dislocation pileups are prone to void nucleation to relax stress concentration. Under tensile stress, microcracks, submicro- and microvoids at strain localization region further grow up to relax stress concentration. As a result, a long crack is formed by crack propagation and coalescence at the location corresponding to the die opening edge, and the material deformed speedily into the die cavity detaches itself from the matrix, so the sheet fractures thoroughly and the plug flies away. Therefore, the process of laser punching can be divided into four stages: high-pressure plasma generation, sheet deformation, crack initiation and growth, and plug formation and dispersion, as shown in Fig. 10.

Similar to the laser shock processing [30, 31], a large amount of energy from the shock wave is imparted into workpiece. Herein, it pushes metal sheet into the die cavity with a high velocity. According to the previous references [22, 32], the initial deformed velocity is proportional to the amplitude of loaded pressure of shock wave, so the velocity of sheet imposed by higher pressure 6.5 GPa is faster than that by the lower pressure 4.5 GPa. The investigations of previous researches demonstrate that the necking is often found at the edge of bulged shape if the higher pressure is applied in laser shocking sheet forming, and the location of necking is corresponding to the die cavity entrance. If the depth of die cavity is deeper than that of the deformed sheet, whether the failure of fracture takes place or not depends on a critical deforming velocity [33, 34]. When the deforming velocity exceeds the critical forming velocity, the fracture arises [32, 35]. Under the higher pressure, the material strain rate is higher, and the punching time is shorter. The sheet in the die opening doesn't have enough time to deform fully, and the cracks have no sufficient time to grow along the zigzag path. As a result, the plug is flatter, and the edge of the punched hole is smoother. Therefore, the quality of hole punched by the higher peak pressure is superior to that punched by the lower one. Due to the rupture complexity induced by the laser-induced shock wave, the fracture mechanism needs further investigations in the future.

7 Conclusions

1. The process of laser punching mainly includes four stages, high-pressure plasma generation, sheet deformation, crack initiation and growth, and plug flying away.
2. The time to complete punching the sheet with higher peak pressure of shock wave is shorter than that with lower pressure.
3. The height of plug punched by higher peak pressure is lower than that punched by the lower one.
4. The edge of the punched hole resulted from the higher peak pressure of shock wave is smoother than that from the lower one, and the quality of hole fabricated by the higher pressure is superior.

Funding information The authors greatly appreciate the support from the National Natural Science Foundation of China (Grant nos. 51675002, 51175002), the Natural Science Foundation of Anhui province (Grant no. 1708085ME110), Huazhong University of Science and Technology (Grant no. P2017-007), and the Open Foundation of Zhejiang Provincial Top Key Academic Discipline of Mechanical Engineering (Grant no. ZSTUME02A05).

Compliance with ethical standards

Conflict of interest The authors declare that they have no conflicts of interest.

References

1. Cheng GJ, Pirzada D, Ming Z (2007) Microstructure and mechanical property characterizations of metal foil after microscale laser dynamic forming. J Appl Phys 101(6):063108
2. Wielage H, Vollertsen F (2009) Investigations of forming behaviour in laser shock forming. Steel Res Int 80(5):323–328
3. Lambiase F, Llio AD, Paoletti A (2016) Productivity in multi-pass laser forming of thin AISI 304 stainless steel sheets. Int J Adv Manuf Technol 86(1–4):259–268
4. Shahabad SI, Naeini HM, Roohi AH, Soltanpour M, Tavakoli A (2017) Height prediction of dome-shaped products in laser forming process. Int J Adv Manuf Technol 88(5–8):2227–2236
5. Ding HT, Pence C, Ding H, Shen NG (2013) Experimental analysis of sheet metal micro-bending using a nanosecond-pulsed laser. Int J Adv Manuf Technol 69(1–4):319–327
6. Cheng JG, Zhang J, Chu CC, Zhe J (2005) Experimental study and computer simulation of fracture toughness of sheet metal after laser forming. Int J Adv Manuf Technol 26(11–12):1222–1230
7. Li J, Gao H, Cheng GJ (2010) Forming limit and fracture mode of microscale laser dynamic forming. J Manuf Sci Eng Trans ASME 132(6):061005
8. Zheng C, Sun S, Song LB, Zhang GF, Luan YG, Ji Z, Zhang JH (2013) Dynamic fracture characteristics of $Fe_{78}Si_9B_{13}$ metallic glass subjected to laser shock loading. Appl Surf Sci 286:121–125
9. Liu HX, Wang HJ, Shen ZB, Huang ZH, Li W, Zheng YY, Wang X (2012) The research on micro-punching by laser-driven flyer. Int J Mach Tools Manuf 54-55:18–24
10. Liu HX, Shen ZB, Wang X, Wang HJ (2009) Numerical simulation and experimentation of a novel laser indirect shock forming. J Appl Phys 106(6):063107
11. Zhou JZ, Zhang XQ, Zhang YK, Gu YY, Yang CJ, Ni MX (2006) Hole-forming method and device based on laser shock wave technology. CN, ZL200610039505.4 A
12. Pimenov DY, Guzeev VI (2017) Mathematical model of plowing force to account for flank wear using FME modeling for orthogonal cutting scheme. Int J Adv Manuf Technol 89(9–12):3149–3159
13. Liu JF, Long Y, Ji Z, Zhong MS, Liu Q (2017) The influence of liner material on the dynamic response of the finite steel target subjected to high velocity impact by explosively formed projectile. Int J Impact Eng 109:264–275
14. Yasar M, Demirci HI, Kadi I (2006) Detonation forming of aluminum cylindrical cups experimental and theoretical modelling. Mater Des 27(5):397–404
15. Quan HT, Champliaud H, Feng ZK, Dao TM (2014) Analysis of the asymmetrical roll bending process through dynamic FE simulation and experimental study. Int J Adv Manuf Technol 75(5–8):1233–1244
16. Zheng C, Zhang X, Liu Z, Ji Z, Yu X, Song LB (2018) Investigation on initial grain size and laser power density effects in laser shock bulging of copper foil. Int J Adv Manuf Technol 96(1–4):1483–1496
17. Buchely MF, Maranon A, Silberschmidt VV (2016) Material model for modeling clay at high strain rates. Int J Impact Eng 90:1–11
18. Ramajeyathilagam K, Vendhan CP, Rao VB (2001) Experimental and numerical investigations on deformation of cylindrical shell panels to underwater explosion. Shock Vib 8(5):253–270
19. Škrlec A, Klemenc J (2016) Estimating the strain-rate-dependent paramaters of the Cowper-Symonds and Johnson-cook material models using taguchi arrays. Stroj Vestn 62(4):220–230
20. Zhao SG, He Z, Yang JL, Cheng W (2007) Experiment investigation of dynamic material property of aluminium alloy. J Beijing Univ Aeronaut Astronaut 33(8):982–985
21. Fabbro R, Fournier J, Ballard P, Devaux D, Virmont J (1990) Physical study of laser-produced plasma in confined geometry. J Appl Phys 68(2):775–784
22. Zhang XQ, She JP, Li SZ, Duan SW, Zhou Y, Yu XL, Zheng R, Zhang B (2015) Simulation on deforming progress and stress evolution during laser shock forming with finite element method. J Mater Process Technol 220:27–35
23. Rosenberg Z, Dekel E (2009) Terminal ballistics. Springer, Berlin
24. Du WW, Wang L, Zhao DH, Zhi MS, Xu X (2015) Study of the dynamic behaviors of Ti-5553 alloy based on Taylor bar impacting test. Acta Armamentarii 36(9):1750–1756
25. Xiao XK, Zhang W, Wei G, Mu ZC, Guo ZT (2011) Experimental and numerical investigation on the deformation and failure behavior in the Taylor test. Mater Des 32(5):2663–2674
26. ABAQUS (2010) Theory manual version 6.10, dassault system
27. Zhang XQ, Zhang Y, Zhang YW, Pei SB, Huang ZL, Deng L, Li SZ (2018) Numerical and experimental investigation of laser shock forming aluminum alloy sheet with mold. Int J Mater Form 11(1):101–112
28. Shehadeh MA, Zbib HM, Rubia TDDL (2005) Modelling the dynamic deformation and patterning in fcc single crystals at high strain rates: dislocation dynamic plasticity analysis. Philos Mag 85(15):1667–1685
29. Wielage H, Vollertsen F (2011) Classification of laser shock forming within the field of high speed forming processes. J Mater Process Technol 211(5):953–957
30. Zhang XQ, Chen LS, Li SZ, Duan SW, Zhou Y, Huang ZL, Zhang Y (2015) Investigation of the fatigue life of pre- and post-bone specimen subjected to laser shot peening. Mater Des 88:106–114
31. Irizalp SG, Saklakoglu N, Yilbas BS (2014) Characterization of microplastic deformation produced in 6061-T6 by using laser shock processing. Int J Adv Manuf Technol 71(1–4):109–115
32. Li J, Cheng GJ (2010) Multiple-pulse laser dynamic forming of metallic thin films for microscale three dimensional shapes. J Appl Phys 108(1):013107
33. Hu XY, Daehn GS (1996) Effect of velocity on flow localization in tension. Acta Mater 44(3):1021–1033
34. Karman TV, Duwez P (1950) The propagation of plastic deformation in solids. J Appl Phys 21(10):987–994
35. Xiao XK, Zhang W, Wei G, Mu ZC (2010) Effect of projectile hardness on deformation and fracture behavior in the Taylor impact test. Mater Des 31(10):4913–4920